Ex vivo photoacoustic nodal metastases detection in a rat model using a clinical superparamagnetic iron oxide nanoparticle dispersion

Diederik J. Grootendorst[1], Raluca M. Fratila[2], Martijn Visscher[2], Bennie Ten Haken[2], Richard van Wezel[3], Sven Rottenberg[4], Wiendelt Steenbergen[1], Srirang Manohar[1] and Theo J. M. Ruers[4]

Short abstract (100 words)
Detection of tumor metastases in the lymphatic system is essential for intra-operative staging of various malignancies. Pre-operative injection of clinically approved superparamagnetic iron oxide (SPIO) nanoparticles has been shown to improve MRI based nodal staging. The application of a clinical grade SPIO dispersion is verified by photoacoustically imaging *ex vivo* nodes from a metastatic animal model. Results were compared with 14 Tesla MR images and histology.
In metastatic nodes, larger and smaller irregularities were observed in the normally homogeneous SPIO distribution while overall PA signal was decreased throughout the node. Irregularities could be correlated to the absence of contrast in the MR images and linked to metastatic deposits seen on the histological slides. The results pave the way for a clinical evaluation of the technique.

Background
Detection of tumor metastases in the lymphatic system is essential for accurate staging of various malignancies, however fast and accurate intra-operative evaluation of the nodal status remains difficult to perform with common available medical imaging techniques. Photoacoustic (PA) imaging shows potential in this regard, but requires the use of extraneous contrast for visualization. In recent years, numerous studies have confirmed the additional value of superparamagnetic iron oxide dispersions (SPIOs) for nodal staging purposes, prompting the clearance of different SPIO dispersions for clinical practice. Here we evaluate whether a combination of PA imaging and a clinically approved SPIO dispersion, could have the potential for sensitive assessment of the nodal status intra-operatively.

Materials and methods
Prostate adenocarcinoma cells (MAT-lylu) were inoculated in the footpad of Copenhagen rats. For lymph node imaging, the animals received a subcutaneous injection of a SPIO dispersion (Endorem, Guerbet, France) either 5 or 8 days after tumor inoculation. The resected nodes were photoacoustically imaged at 720 nm using 20 mJ/cm^2, 24 hours later and imaging results were compared to 14 Tesla MR imaging and histology. The SPIO amount was also quantified using Vibrating Sample Magnetometry and correlated to the amount of PA contrast. Control nodes were obtained from the contra lateral side of the inoculated leg with and without previous SPIO injections.

Results
Control nodes showed homogeneous contrast bands containing high PA intensities in their peripheral zone. A similar distribution was observed by MRI. In the tumor groups, larger and smaller irregularities were observed in the homogeneous distribution and the overall PA signal was decreased

[1] Biomedical Photonic Imaging Group, MIRA Institute for Biomedical Technology and Technical Medicine, Faculty of Science and Technology, University of Twente, P.O. Box 217, 7500 AE Enschede, The Netherlands.
[2] Neuro IMaging group, MIRA Institute for Biomedical Technology and Technical Medicine, Faculty of Science and Technology, University of Twente, P.O. Box 217, 7500 AE Enschede, The Netherlands
[3] Neurophysiology, Donders Institute for Brain, Cognition and Behaviour, Radboud University Nijmegen, P.O. Box 9104, 6500 HE Nijmegen, The Netherlands
[4] Netherlands Cancer Institute - Antoni van Leeuwenhoek Hospital (NKI-AVL), The Netherlands;
Also at Nanobiophysics Group, MIRA Institute for Biomedical Technology and Technical Medicine, Faculty of Science and Technology, University of Twente, P.O. Box 217, 7500 AE Enschede, The Netherlands.
+31205122565, t.ruers@nki.nl
Dr. Van Leeuwen, Dr. Manohar and Dr. Steenbergen have a minor interest in PA Imaging BV, which however did not finance the research in any way. All other authors declare to have no conflict of interest.

throughout the node. The irregularities could be correlated to the absence of contrast in the MR images and could be linked to metastatic deposits seen on the histological slides

Conclusions
We conclude that the combination of photoacoustic imaging with a clinically approved iron oxide nanoparticle dispersion is able to detect lymph node metastases in resected lymph nodes. This approach opens up new possibilities for intra-operative nodal staging.

Introduction

Metastases in the lymphatic system are a predictor of poor outcome in many solid malignancies [1-4] and is signaled out as one of the greatest challenges in cancer treatment today. The presence of lymph node metastases decreases the 5-year survival of melanoma patients, independent of other prognostic factors of the primary tumor [5]. Likewise, the number of metastatic lymph nodes resected correlates with survival in breast cancer patients [6]. Despite the importance of lymph node metastases as highlighted by its inclusion in cancer staging systems, both early detection and treatment remains far from optimal.

Superparamagnetic iron oxide nanoparticle (SPIO) enhanced MRI has been proven to detect small and otherwise undetectable lymph-node metastases in patients with prostate cancer [7], providing a possibility to improve early diagnosis and decision making. In addition, this approach has also been proven to be of additional benefit for head and neck, breast and pelvis lymph node assessment showing a overall sensitivity of 88% and an overall specificity of 96% based on 19 prospective studies [8]. After subcutaneous or intravenous injection, SPIOs are cleared by draining lymphatic vessels and transported to the regional lymph nodes where they are phagocytosed by nodal macrophages. Inhomogeneties in SPIO uptake arise once metastatic cells displace the normal nodal architecture which can be visualized by MRI due to the changes in relaxations time. This metastases detection scheme is schematically displayed in Figure 1.
Although, MRI is not able to detect micrometastases of less than 1 mm using a conventional 1.5 Tesla system [9], the success of the approach together with the fact that coated SPIOs contain a satisfactory safety profile for human applications [10] have cleared several SPIO dispersions for clinical use.

Photoacoustic (PA) imaging, an emerging powerful optical imaging modality using optical absorption contrast and ultrasonic resolution, is being widely applied within biomedical research [11, 12]. PA imaging relies on the detection of acoustic waves produced by the thermoelastic expansion of tissue following absorption of short pulsed optical illumination. By this mechanism, PA uncouples signal generation and detection, enabling diffused photons to also contribute to the resultant PA signals without degrading the signal quality. In addition, in biological tissue, ultrasonic scattering is about two to three orders of magnitude weaker than optical scattering, resulting in high spatial resolution compared to many optical techniques. The fact that PA imaging, makes no use of ionizing radiation and enables fast imaging performance, could facilitate its introduction as an additional medical imaging technique.

PA imaging can both be based on endogenous biomolecules with natural PA contrast properties (e.g. hemoglobin, melanin), or exogenous contrast agents delivered by injection. The strong PA response of many endogenous biomolecules enables the detection of melanoma cells [13, 14] and melanoma metastases [15, 16] or, for example, the visualization of the vasculature associated with breast carcinoma [17-19]. Exogenous contrast agents, on the other hand, are mostly applied to enhance biological processes which lack an endogenous biomolecule related to the studied disease state, including many malignancies [20-22]. To this end, multiple exogenous contrast agents are subject to extensive research to analyze their benefit in the monitoring of specific disease states. Various nano-materials have been used *in vivo* to investigate the lymphatics using different optical techniques, whereby the contrast agent is absorbed and transported from the interstitial tissue into the collector lymphatics after interstitial injections [23, 24]. In order to increase the imaging depth while maintaining a high spatial resolution, PA imaging could be of additional value. Research into the PA imaging of the lymphatics using nano-materials is however, more limited and is mostly centered

around the mapping of the sentinel lymph node(s) (SLN(s)) [25-28]. Recently, Akers *et al.* visualized the SLN of rats after methylene blue injection and verified their results using SPECT/CT [29]. Pan *et al.* proved that copper nanoparticles can be used to enhance and visualize SLN(s) *in vivo* using PA imaging [30].

While showing promising results, most PA exogeneous contrast agents require an extensive approval procedure to be admitted for clinical use by the Food and Drugs Administration (FDA) or European Medicines Agency (EMA). SPIOs on the other hand are cleared for clinical use and the lymphatic metastasis detection potential of SPIOs as verified by several clinical MRI studies [7, 8] makes them potentially valuable for intra-operative lymph node staging. Not only could *in vivo* nodal staging provide a diagnostic benefit for the surgical team but a compact PA device could possibly also be used to stage *ex vivo* nodes, resulting in the direct availability of pathological information in the operation room. This approach is already under investigation for several other optical techniques like OCT [31] and Raman spectroscopy [32], both showing clear potential, but has not been attempted for photoacoustics. In order to explore this concept, our group recently injected clinical SPIO dispersions in healthy rodents to verify whether these deposits could be detected with PA and showed that the distribution of SPIOs could be mapped with accuracy down to an amount of ±11 µg [33]. Although, this demonstrated the technical feasibility of the approach, the applicability of SPIOs for distinguishing benign from metastatic lymph nodes was not analyzed. In order to pave the way for a clinical evaluation, it therefore remains to be verified whether (smaller) nodal metastases can be detected using this approach. In this work, we validate the potential of a clinically approved SPIO dispersion (Endorem®) for the detection of nodal metastases in resected nodes using a metastatic animal model and correlate the results with MRI and histology. In addition, we quantify the SPIO PA response within the nodes and compare it to measured iron amounts. In the future, these results could possibly lead to a rapid clinical introduction of a PA based technique for intra-operative applications.

Materials and Methods

Animal model and tumor cell line

To study the possibility of photoacoustic lymph node assessment using SPIOs, female Copenhagen rats, weighing 150-200 g were subcutaneously injected with R3327 MAT-lylu cells in their left hindpaw. This model has also been frequently used to validate the potential of SPIO agents in MRI [34, 35]. All experiments were approved by the local Animal Care Committee.
The R3327 MAT LyLu prostate tumor variant has been used as an experimental model for syngeneic progression and metastasis of prostate adenocarcinoma. *In vivo*, this tumor is characterized by a rapid and hormone-independent proliferation, anaplastic histology, and metastases to draining lymph nodes and lungs. Cells were cultured in RPMI-1640 medium, supplemented with 10% fetal calf serum and 100 ml penicillin/streptomycin.

For the experiments, one million R3327 MAT LyLu tumor cells were dispersed in 0.1 mL of medium and inoculated aseptically in eight Copenhagen rats. The animals were separated into two groups of which one was given an subcutaneous injection of 0.1 ml of SPIOs (11.2 g/l) (Endorem, Guerbet, France) in both hindpaws, 5 days after inoculation (minor metastatic group) and one group 3 days later (major metastatic group). Time spans were chosen according to a pilot study which showed that the popliteal lymph nodes were totally replaced by metastatic cells after 12 days and showed initial metastatic involvement after 4 days. Because we aimed to study the changes in SPIO distribution at an earlier stage of metastatic involvement the inoculation time was set at 5 and 8 days.
Twenty-four hours after SPIO injection the animals were euthanized by cervical dislocation and the popliteal lymph nodes of both hindlegs were dissected. Four popliteal nodes of the contra lateral side were used as controls (control group) because research has proven that they remain without metastasis within the used inoculation time [34]. In addition to the two tumor groups, two animals received no SPIO injection after 5 days of inoculation to verify the PA response in metastatic and normal nodes without SPIOs. After PA and MR imaging nodes were embedded in paraffin, cut into 5 µm slices and stained using a normal H&E staining. To visualize the locations of the metastases and compare them with the PA and MR images, one of the nodes was additionally immunohistochemically stained for

vimentin. Vimentin, a type III intermediate filament (IF) protein and mesenchymal marker, is specifically suited to stain poorly differentiated and highly metastatic cells like the MAT-lylu line. Attention was paid during sectioning of the tissue to ensure the orientation corresponded with the imaging plane of both PA as MR imaging.

Photoacoustic imaging setup

Resected nodes were placed inside a hollow transparent 3% Agar sample holder with an inner diameter of 25 mm and wall thickness of 10 mm. Twenty tomographic projections were acquired at approximately 20 mJ/cm^2 using the instrument we described earlier [36]. In summary, the system (Fig. 2) consists of a Q-switched Nd:YAG laser (Brilliant B, Quantel, France) with an optical parametric oscillator (Opotek, 700 to 950 nm) operating at a 10 Hz repetition rate. The light is delivered via a beam expander creating a beam diameter of around 1 cm to cover sample in a top-illumination configuration [37]. The photoacoustic signals are recorded with a curvilinear detector array (Imasonic, Besançon) consisting of 32 elements and shaped to 85º of a circle of 40 mm radius. The center frequency of the array is 6.25 MHz with a reception bandwidth greater than 80%. Individual elements have sizes of 10 by 0.25 mm. These elements are arranged with an inter-element spacing of 1.85 mm. At each position signals are acquired from the detector using a 32 channel pulse-receiver system (Lecoeur Electronique, Paris, France) with a sampling rate of 80 MHz. Filtered acoustic backprojection was used to reconstruct the PA images. Images were acquired using an excitation wavelength of 720 nm. While 720 nm is not an exclusive wavelength for detecting SPIO's, it combines a low absorption of total hemoglobin with a significant absorption of the SPIO dispersion, while absorption by fat (and water) remains negligible [38]. In addition, it allows for a direct comparison with our previous results in healthy animals [33]. Image slice acquisition time of the system for 20 projections is about 60 seconds.

In addition to the single wavelength illumination at 720 nm, multiple wavelength images of two lymph nodes were acquired at 720, 740, 760 and 780 nm. Multiple wavelength information could possibly facilitate the distinction of the SPIO deposits from other biological absorbers in an *in vivo* setting. To this end, average pixel value of the PA contrast regions within the images was calculated and compared to spectroscopic values of the SPIO dispersion. For comparison, both the spectroscopic data and the average pixel values within the images were normalized.

Magnetic Resonance Imaging

In order to achieve a comparable spatial resolution to our PA images, the nodes were imaged using the 14 Tesla MRI system (Bruker, Ettlingen, Germany) described earlier [33]. Before imaging the nodes were transferred to quartz NMR tubes with a diameter of 10 mm and fixated using 4% buffered formaldehyde. All nodes were positioned according to the orientation in the PA setup. A Multi-slice-multi-echo (MSME) imaging sequence was used with an echo time of 10 ms and a repetition time of 1000 ms. The sequence produces a larger longitudinal and transverse magnetization making the surrounding fat appear bright, facilitating nodal identification and SPIO distribution analysis in the imaged volume. Images were acquired using a matrix dimension of 256x256, a field of view of 1 cm, 25 averages and a slice thickness of 1 mm. MR scan time mounted up to 2 hours per node.

Contrast quantification

The amount of iron inside the lymphatic tissue was quantified with a vibrating sample magnetometer (VSM) (Quantum Design, San Diego, United States) with a variable magnetic field of ± 4 Tesla. From the measured SPIO amounts a concentration estimation ($\mu g/mm^3$) within each node was calculated by dividing the total iron amount by the volume of the node. Nodal volume was extracted from the dimensions of the MR images. The estimated concentration was then correlated to the amount of PA contrast within each nodal image by manually selecting the nodal area within the PA image and calculating the average pixel value of the selection. To exclude large deviations in single pixel values, a 5x5 pixel moving average was first implemented on each PA image. Due to the fact that the detector contains an image slice thickness of approximately 1 mm, the average pixel value (AVP) of each selected image region was then divided by its area to produce a "contrast" concentration (AVP/mm^3) comparable with the estimated iron concentration.

Results

A comparison between the PA and MR images for the different animal groups is shown in Figure 3-5. PA imaging of lymph nodes without an exogeneous contrast agent both benign and malignant (Fig. 3) shows that almost no PA response is generated by nodal tissue without the SPIO additive and no clear structures can be distinguished. As a result no clear distinction can be made between nodes with and without metastases. Such a distinction can also not be made based on the corresponding unenhanced MR images. The absence of hypo-intense regions also indicate that no SPIO particles are present within the nodal volume.

The control group (Fig. 4) shows that addition of the SPIOs results in a clear and continuous ring of PA contrast in the peripheral zone of the nodes. The ring like patterns are relatively free of intermissions and show significantly large PA responses throughout their volume compared to the background. The associated MR images contain blackening throughout the nodal volume with no exception of the nodal centre except for the third node (Fig. 4(3), red arrow). The contrast bands are also free of any large irregularities and seem to display an uniform distribution within the nodes. Shapes and dimensions correspond for both imaging modalities. The detected iron concentrations measured with VSM varies from 2.9 to 4.2 $\mu g/mm^3$ (Table 1). Histology reveals no metastatic cells (Fig. 6(1-3)).

The PA images of the nodes in the major metastatic group (Fig. 5(1-4)) show an altered contrast distribution without the presence of a continuous contrast band and a lowered PA response. The PA signal areas within the images display a discontinuous, irregular distribution with a decreased PA signal response compared to the control nodes (Table 1). MR images show a similar contrast distribution with a lack of increased relaxation in large areas of the nodal volume (Fig. 5, red arrows). In areas displaying the presence of SPIO contrast, the contrast bands seem to be irregular with spots lacking hypo-intensity within these contrast areas. Again there is a clear resemblance in contrast distribution between the MR and PA images, as more clearly displayed by a comparison of the images of lymph node 1 (Fig. 7). Both maps show a similar lack of contrast in the left lower part of the node while an irregular contrast band is located in the upper right. The iron concentration measured within the nodes of the major metastatic group is also significantly lower compared to the control group with concentrations ranging from 0.4 to 1.0 $\mu g/mm^3$ (Table 1). Histology reveals the presence of metastatic cells (Fig. 6(4-6)) in all nodes, although the location of these metastases could not to be matched to all contrast lacking areas in the MR or PA images on a point-to-point basis. This is more clear once the images of lymph node 1 are compared to the vimentin stains (Fig. 7). Although the node shows larger metastatic deposits in the lower peripheral zone of the node (red arrows) compared to the upper part (blue arrows), the vimentin map shows that not all contrast lacking areas correspond to metastatic cell deposits.

The PA images of the nodes in the minor metastatic group (Fig. 5(5-8)) do also display irregularities in their contrast distribution and a decreased PA response per mm^3 (Table 1). The amount of PA contrast per mm^3 has however decreased less than within the major metastatic group (Table 1). The corresponding MR images also show areas which lack the hypo-intensity caused by SPIO presence (Fig. 5, purple arrows) and to great extent correlate to the absorption patterns of the PA images. However, the hypo-intense areas seem to be less extensively present than within the major metastatic group. Compared to the other nodes within the group, lymph node 6 displays a more regular contrast distribution with only a minor area of SPIO absence in the left peripheral zone (purple area). Measured iron concentrations lie between the control and major metastatic group ranging from 1.1 to 1.8 $\mu g/mm^3$ (Table 1.).

Correlation of the measured iron concentrations with the calculated AVPs using the least squares approach reveals a strong linear relation between the two (Fig. 8), revealing a correlation coefficient (CC) of 0.94 and a corresponding root mean square of the error (Root MSE) of 1.3. This correlation shows that it could be possible to produce an estimation of the iron concentration by analyzing the PA image contrast within the node. Multiple wavelength imaging of SPIO containing areas in two of the lymph nodes shows an almost constant average PA response for 720, 740, 760 and 780 nm excitation. This constant response accords with the extinction spectrum of the SPIO dispersion which shows larger optical extinction at shorter excitation wavelengths (Fig. 9).

Discussion

The results demonstrate that there is a difference in both the PA contrast pattern and the PA intensity between resected rat lymph nodes with and without metastatic deposits. A regular high intensity PA contrast pattern in the periphery of the nodes seems to correspond to an absence of nodal metastases while the presence of metastatic deposits results in a decline of PA signal intensity and irregularization of PA contrast band. MR imaging shows a similar phenomenon with the presence of larger areas of hyper-intensity once the tumor inoculation time is prolonged. These findings correspond with the general theory of SPIO uptake in benign and malignant lymph nodes which is altered due to displacement of pheripheral macrophages by metastatic cells as explained by Kimura *et al* [39]. To our understanding this is the first time that nodal metastases are visualized with PA imaging using a non-specific clinically approved contrast nanoparticle. However, the vimentin staining (Fig. 7) shows that both PA and MRI do not produce an one-on-one map of the metastatic cell deposits because benign and malignant cells are also depicted at other locations within the node. This could be explained by small differences in orientation or the fact that MRI and PAI contain slice thicknesses of 1 mm while histological slides are only 5 µm. However, it could also be caused by the influence of metastatic cells on the phagocytic uptake. Because this influence is largely unknown, it could be speculated that even if lymphocytes are not totally displaced by metastatic cells, their uptake is somewhat altered due to the presence of metastatic deposits. This could mean that even if histology shows solitary metastatic cell deposits the SPIO uptake could be reduced in that part of the node. This leads us to conclude that PA images should not be viewed as an exact metastatic map, but that alterations in the absorption pattern should be interpreted as indications of metastatic involvement within the nodal volume. Although this might decrease the eventual sensitivity of the technique it could hold enough distinguishing power to be applied as an rapid screening application within an intra-operative setting.

In contrast to the indication that a regular PA contrast distribution combined with a high signal intensity seems to correspond to a healthy node, one of the metastatic nodes, namely number 6, also shows a relatively regular and intensive PA band. The absence of contrast in the lower left part of the node (purple arrow) represents the only irregular observation in both PAI and MRI, making it challenging to define to which extent metastases have to be progressed before they can be sensitively detected with this approach. Additional research on lymph nodes harboring early metastatic involvement could provide more information whether in most cases the metastatic induced phagocytotic changes will result in detectable alterations of the PA contrast map and how this has impact on the sensitivity and specificity of the technique.

The MR and PA images show clear similarities in the distribution of SPIO contrast, indicating that SPIO distributions can also be accurately mapped using photoacoustics. With regard to image quality the MRI system is superior compared to the tomographic PA system but it has to be taken into account that MR image acquisition time is several hours. Furthermore, a comparable MR setup is not only expensive and bulky but also contains a strong magnetic field which is unsuitable for an intra-operative setting. These advantages emphasize the possible additional benefit of a PA approach.
The decrease in PA intensity within the metastatic nodes corresponds to a measured decrease in iron concentration (Table 1). The iron concentrations measured with VSM show a decline in SPIO uptake depending on the length of the primary tumor inoculation time. PA contrast amounts are shown to have a strong linear relationship (CC: 0.94) with the iron concentrations indicating that the PA intensity could be converted into an estimation for the iron amount. Although this remains to be a qualitative estimation because the actual photon fluence within the tissue is unknown, more quantitative approaches could possibly be implemented using an ultrasound modulated fluence correction approach [40]. For now, the fact that PA intensity per mm^3 seems to be decreased in metastatic nodes which can be linked to a decreased iron concentration, shows that PA intensity measurements could possibly be used as an additional tool for nodal assessment.

The fact that the control lymph nodes are smaller and contain less immune cells than the nodes within the tumor groups could raise some questions about the applicability of the technique for large reactive nodes. These nodes could for example be present once the immune systems reacts to the presence of a primary tumor. Although, we stress the importance of further research, results in a healthy animal model in which reactive nodes were induced by incomplete Freund Adjuvant injection also showed the

presence of regular high intensity peripheral PA contrast bands [33]. This seems to indicate that the uptake of SPIOs by the peripheral macrophages is unaltererd even if, tumor induced reactivity results in the presence of more immune cells and swelling of the node. The technique might therefore also be suitable for larger or activated lymph nodes.

Finally, even though the results demonstrate the potential of an intra-operative PA application for resected nodal scanning, the use of SPIOs in an *in vivo* setting could also be considered. In such a setting, the fact that smaller SPIO deposits generate inferior PA response [41] could be compensated by differentiation on the basis of multiple wavelength excitation. The constant PA response of the SPIOs in the near-infrared (Fig. 9) is dissimilar from the varying absorption of oxy- and deoxyhemoglobin, providing some grounds to separate the PA signals of both. Future research, will be directed towards such a spectral method which should verify if SPIOs contain *in vivo* applicability.

Conclusion

The use of a tomographic PA setup together with a clinically approved SPIO dispersion is capable of distinguishing benign from malignant nodes in an *ex vivo* setting. Indications for metastatic involvement seem to be a lowered and irregular PA intensity pattern which can be linked to a decreased SPIO concentration and distribution. These results pave the way for a clinical exploratory study into the accuracy of the technique for intra-operative staging.

Acknowledgements

We acknowledge the contribution of dr. J. Jose for his insights in the photoacoustic imaging procedure and thank Ms. B. Klomphaar for her help regarding animal care. Additionally we thank the experimental urology department of the Radboud University Nijmegen for generously supplying us with the MAT-lylu cell line. The work was funded by the MIRA institute for Biomedical Technology and Technical Medicine.

1. Govindarajan A, Baxter NN: Lymph node evaluation in early-stage colon cancer. *Clin Colorectal Cancer* 7(4), 240-246 (2008).
2. Giuliano AE, Kirgan DM, Guenther JM, Morton DL: Lymphatic mapping and sentinel lymphadenectomy for breast cancer. *Ann Surg* 220(3), 391-398; discussion 398-401 (1994).
3. Morton DL, Wen DR, Wong JH *et al.*: Technical details of intraoperative lymphatic mapping for early stage melanoma. *Arch Surg* 127(4), 392-399 (1992).
4. Liptay MJ: Sentinel node mapping in lung cancer. *Ann Surg Oncol* 11(3 Suppl), 271S-274S (2004).
5. Balch CM, Soong SJ, Gershenwald JE *et al.*: Prognostic factors analysis of 17,600 melanoma patients: validation of the American Joint Committee on Cancer melanoma staging system. *J Clin Oncol* 19(16), 3622-3634 (2001).
6. Krag DN, Single RM: Breast cancer survival according to number of nodes removed. *Ann Surg Oncol* 10(10), 1152-1159 (2003).
7. Harisinghani MG, Barentsz J, Hahn PF *et al.*: Noninvasive detection of clinically occult lymph-node metastases in prostate cancer. *N Engl J Med* 348(25), 2491-2499 (2003).
8. Will O, Purkayastha S, Chan C *et al.*: Diagnostic precision of nanoparticle-enhanced MRI for lymph-node metastases: a meta-analysis. *Lancet Oncol* 7(1), 52-60 (2006).
9. Taupitz M, Wagner S, Hamm B: Contrast media for magnetic resonance tomographic lymph node diagnosis (MR lymphography). *Radiologe* 36(2), 134-140 (1996).
10. Clement O, Siauve N, Cuenod CA, Frija G: Liver imaging with ferumoxides (Feridex): fundamentals, controversies, and practical aspects. *Top Magn Reson Imaging* 9(3), 167-182 (1998).
11. Wang LV, Hu S: Photoacoustic tomography: in vivo imaging from organelles to organs. *Science* 335(6075), 1458-1462 (2012).
12. Razansky D, Deliolanis NC, Vinegoni C, Ntziachristos V: Deep tissue optical and optoacoustic molecular imaging technologies for pre-clinical research and drug discovery. *Curr Pharm Biotechnol* 13(4), 504-522 (2012).

13. O'brien CM, Rood K, Sengupta S *et al.*: Detection and isolation of circulating melanoma cells using photoacoustic flowmetry. *J Vis Exp* (57), e3559 (2011).
14. O'brien CM, Rood KD, Bhattacharyya K *et al.*: Capture of circulating tumor cells using photoacoustic flowmetry and two phase flow. *J Biomed Opt* 17(6), 061221 (2012).
15. Jose J, Grootendorst DJ, Vijn TW *et al.*: Initial results of imaging melanoma metastasis in resected human lymph nodes using photoacoustic computed tomography. *J Biomed Opt* 16(9), 096021 (2011).
16. Grootendorst DJ, Jose J, Wouters MW *et al.*: First experiences of photoacoustic imaging for detection of melanoma metastases in resected human lymph nodes. *Lasers in Surgery and Medicine*, (2012).
17. Heijblom M, Piras D, Xia W *et al.*: Visualizing breast cancer using the Twente photoacoustic mammoscope: What do we learn from twelve new patient measurements? *Opt Express* 20(11), 11582-11597 (2012).
18. Ermilov SA, Khamapirad T, Conjusteau A *et al.*: Laser optoacoustic imaging system for detection of breast cancer. *J Biomed Opt* 14(2), 024007 (2009).
19. Kruger RA, Lam RB, Reinecke DR, Del Rio SP, Doyle RP: Photoacoustic angiography of the breast. *Med Phys* 37(11), 6096-6100 (2010).
20. Luke GP, Yeager D, Emelianov SY: Biomedical applications of photoacoustic imaging with exogenous contrast agents. *Ann Biomed Eng* 40(2), 422-437 (2012).
21. Manohar S, Ungureanu C, Van Leeuwen TG: Gold nanorods as molecular contrast agents in photoacoustic imaging: the promises and the caveats. *Contrast Media & Molecular Imaging* 6(5), 389-400 (2011).
22. Lanza GM: Emerging contrast agents for photoacoustic imaging. *Contrast Media Mol Imaging* 6(5), 331 (2011).
23. Ballou B, Ernst LA, Andreko S *et al.*: Sentinel lymph node imaging using quantum dots in mouse tumor models. *Bioconjug Chem* 18(2), 389-396 (2007).
24. Kosaka N, Bernardo M, Mitsunaga M, Choyke PL, Kobayashi H: MR and optical imaging of early micrometastases in lymph nodes: triple labeling with nano-sized agents yielding distinct signals. *Contrast Media Mol Imaging* 7(2), 247-253 (2012).
25. Song KH, Kim C, Maslov K, Wang LV: Noninvasive in vivo spectroscopic nanorod-contrast photoacoustic mapping of sentinel lymph nodes. *Eur J Radiol* 70(2), 227-231 (2009).
26. Song KH, Stein EW, Margenthaler JA, Wang LV: Noninvasive photoacoustic identification of sentinel lymph nodes containing methylene blue in vivo in a rat model. *J Biomed Opt* 13(5), 054033 (2008).
27. Erpelding TN, Kim C, Pramanik M *et al.*: Sentinel lymph nodes in the rat: noninvasive photoacoustic and US imaging with a clinical US system. *Radiology* 256(1), 102-110 (2010).
28. Galanzha EI, Shashkov EV, Spring PM, Suen JY, Zharov VP: In vivo, noninvasive, label-free detection and eradication of circulating metastatic melanoma cells using two-color photoacoustic flow cytometry with a diode laser. *Cancer Res* 69(20), 7926-7934 (2009).
29. Akers WJ, Edwards WB, Kim C *et al.*: Multimodal sentinel lymph node mapping with single-photon emission computed tomography (SPECT)/computed tomography (CT) and photoacoustic tomography. *Transl Res* 159(3), 175-181 (2012).
30. Pan D, Cai X, Yalaz C *et al.*: Photoacoustic sentinel lymph node imaging with self-assembled copper neodecanoate nanoparticles. *ACS Nano* 6(2), 1260-1267 (2012).
31. Mclaughlin RA, Scolaro L, Robbins P, Hamza S, Saunders C, Sampson DD: Imaging of human lymph nodes using optical coherence tomography: potential for staging cancer. *Cancer Res* 70(7), 2579-2584 (2010).
32. Horsnell JD, Smith JA, Sattlecker M *et al.*: Raman spectroscopy - A potential new method for the intra-operative assessment of axillary lymph nodes. *Surgeon* 10(3), 123-127 (2012).
33. Grootendorst DJ, Fratila RM, Visscher M *et al.*: Evaluation of superparamagnetic iron oxide nanoparticles (Endorem) as a photoacoustic contrast agent for nodal image enhancement. *Contrast Media Mol Imaging* [Ahead of Print], (2012).
34. Vassallo P, Matei C, Heston WD, Mclachlan SJ, Koutcher JA, Castellino RA: Characterization of reactive versus tumor-bearing lymph nodes with interstitial magnetic resonance lymphography in an animal model. *Invest Radiol* 30(12), 706-711 (1995).

35. Klerkx WM, Geldof AA, Heintz AP *et al.*: Longitudinal 3.0T MRI analysis of changes in lymph node volume and apparent diffusion coefficient in an experimental animal model of metastatic and hyperplastic lymph nodes. *J Magn Reson Imaging* 33(5), 1151-1159 (2011).
36. Jose J, Willemink RG, Resink S *et al.*: Passive element enriched photoacoustic computed tomography (PER PACT) for simultaneous imaging of acoustic propagation properties and light absorption. *Opt Express* 19(3), 2093-2104 (2011).
37. Lao Y, Xing D, Yang S, Xiang L: Noninvasive photoacoustic imaging of the developing vasculature during early tumor growth. *Phys Med Biol* 53(15), 4203-4212 (2008).
38. Beard P: Biomedical photoacoustic imaging. *Interface Focus* 1(4), 602-631 (2011).
39. Kimura K, Tanigawa N, Matsuki M *et al.*: High-resolution MR lymphography using ultrasmall superparamagnetic iron oxide (USPIO) in the evaluation of axillary lymph nodes in patients with early stage breast cancer: preliminary results. *Breast Cancer* 17(4), 241-246 (2010).
40. Daoudi K, Hussain A, Hondebrink E, Steenbergen W: Correcting photoacoustic signals for fluence variations using acousto-optic modulation. *Opt Express* 20(13), 14117-14129 (2012).
41. Mienkina MP, Friedrich CS, Hensel K, Gerhardt NC, Hofmann MR, Schmitz G: Evaluation of Ferucarbotran (Resovist) as a photoacoustic contrast agent / Evaluation von Ferucarbotran (Resovist) als photoakustisches Kontrastmittel. *Biomed Tech (Berl)* 54(2), 83-88 (2009).

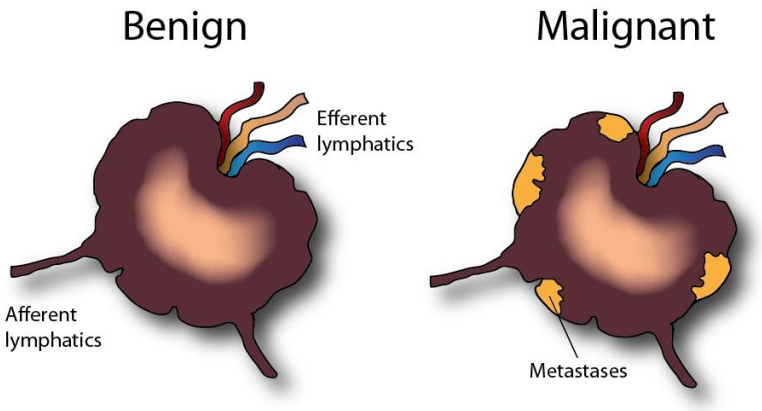

Figure 1. Schematic of the nodal metastases detection scheme using SPIO nanoparticles. In a benign case, the SPIO particles accumulated in a regular pattern in the cortical zone of the lymph node through macrophage uptake 24 hours after injection. Accumulation is mostly centered in the cortical zone of the node due to the particle size of the SPIO agent. In a malignant case, homogenous distribution of the particles is disrupted in locations where metastatic cells have replaced normal nodal architecture. These irregularities can be visualized with MRI due to differences in relaxation times between nodal tissue with and without SPIOs.

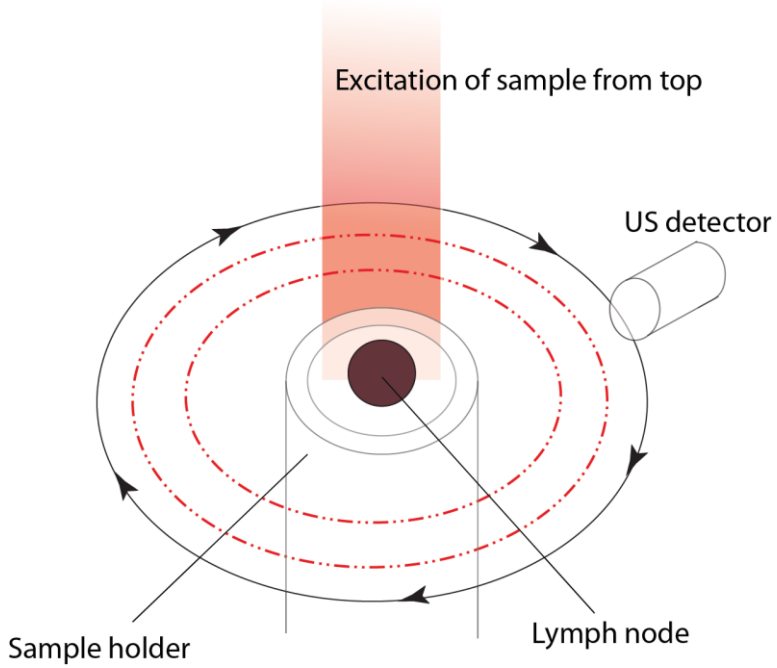

Figure 2. Schematic of the photoacoustic setup. Lymph node samples are placed inside an agar holder and illuminated from the top while the ultrasound detector is rotated around the sample. The entire setup is placed inside a water filled tank to enable wave propagation.

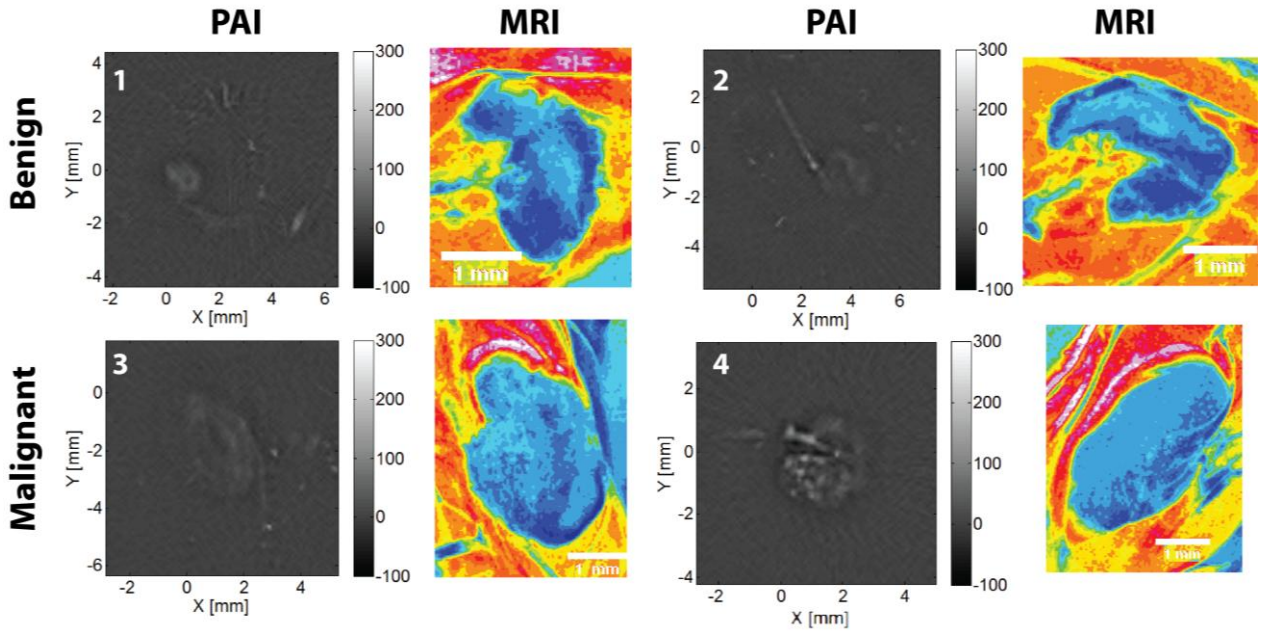

Figure 3. Comparison between PA and MR images of benign and malignant nodes without SPIOs. The PA contrast between the tissue and the background is small and the nodes are not easily distinguished. The MR images show no increased relaxation, corresponding with the absence of SPIOs.

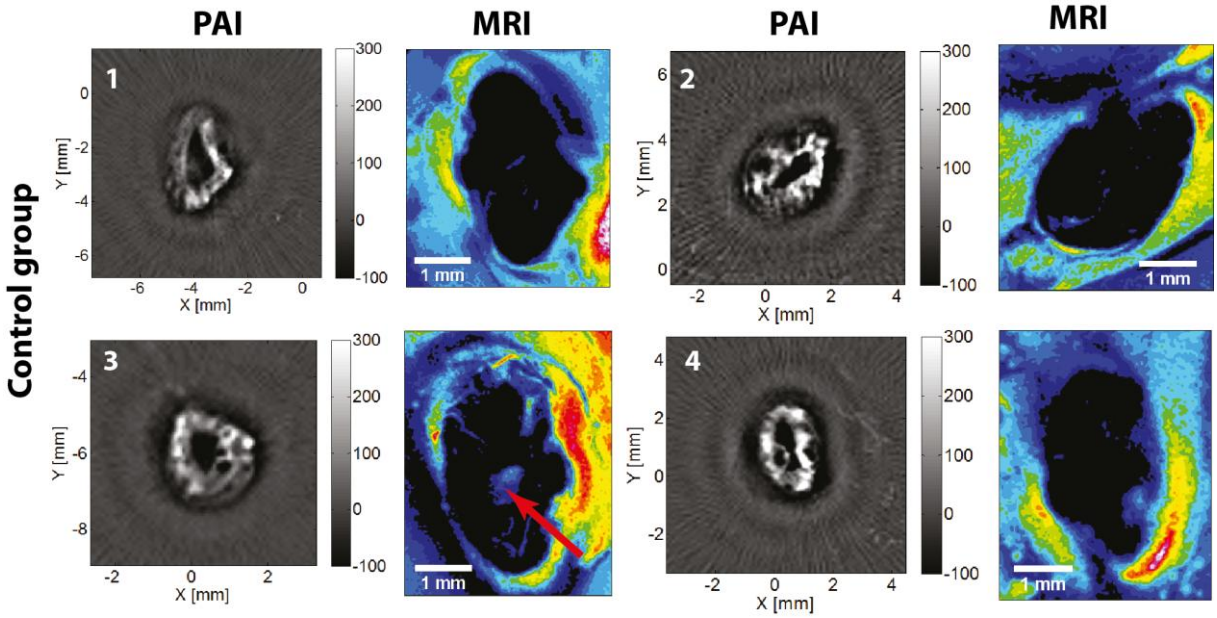

Figure 4. Comparison between the PA and MR images of the control group. The PA images show a clearly distinguishable continuous high contrast band in the peripheral zone of the nodes. MR images show a comparable result with clear signal relaxation (blackened areas) throughout the nodal volume.

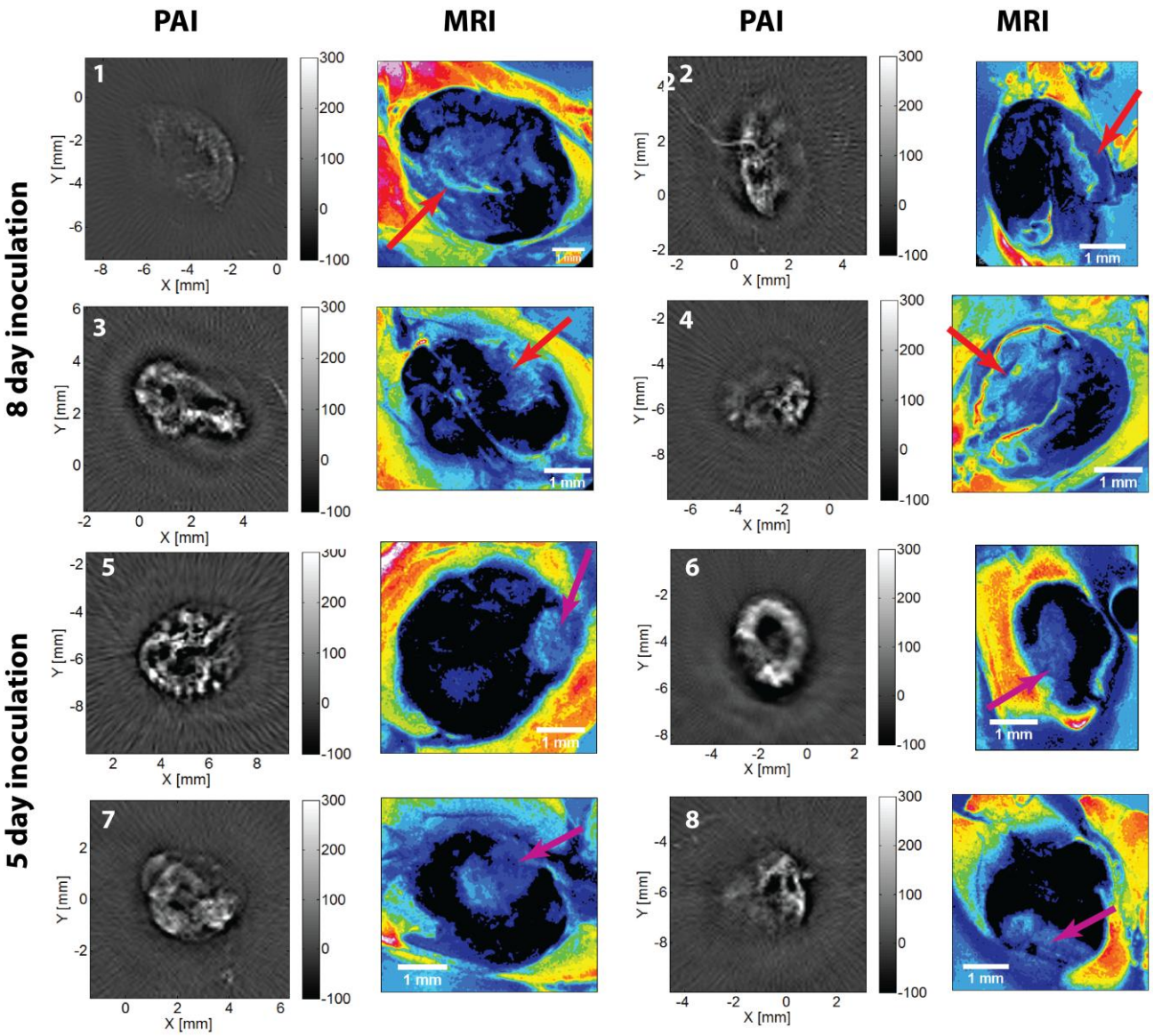

Figure 5. Comparison between PA and MR images of the metastatic groups. The PA response pattern is grossly comparable to the areas of MR signal decrease in all the nodes. The contrast distribution is irregular compared to the control group with large areas lacking enhancement, especially in the major metastatic group (Red arrows). MR and PA contrast patterns grossly compare for all the nodes. In contrast to the other nodes, node 6 seems to contain a regular peripheral contrast band with only a small decreased PA response in the lower left quadrant (purple arrow).

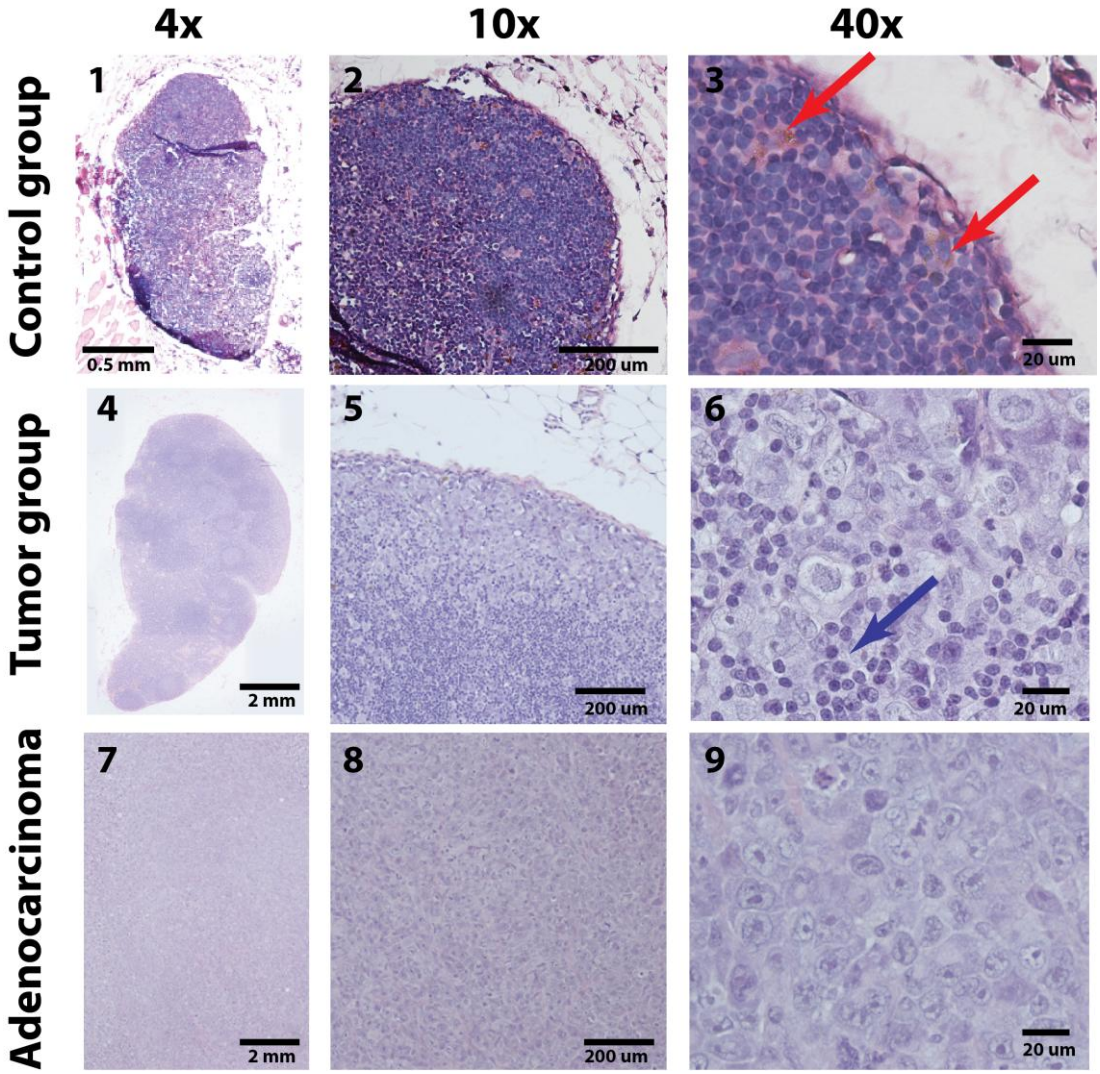

Figure 6. H&E staining of control and tumor group together with the primary tumor at 4x, 10x and 40x magnification. The control nodes show the presence of both lymphocytes and macrophages (1-3). SPIO deposits can be seen within the peripheral zone of the node (red arrows). The nodes in the tumor group show metastatic involvement throughout the nodal volume with larger metastatic deposits in the pheripheral zone (4-6). Normal lymphocytes can still be located near the metastatic areas (blue arrow). The metastasic cells correlate well to the poorly differentiated adenocarcinoma cells of the primary tumor (7-9).

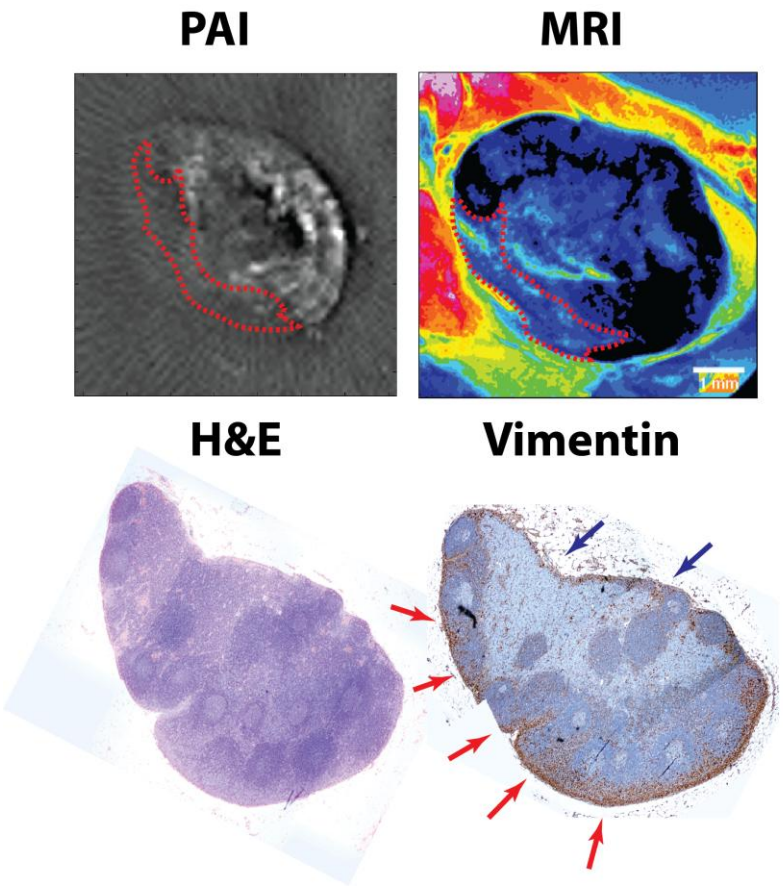

Figure 7. Comparison of PAI and MRI with both H&E and Vimentin histology staining for node 1. - The contrast distribution between PAI and MRI is comparable, showing some SPIOs deposits in the upper parts of the node and absence of SPIOs in the lower parts (Red dotted line). Localization of the metastatic deposits is difficult to correlate to the images using the H&E staining due to lack of contrast between metastatic cells and lymphocytes. Vimentin staining shows the metastatic deposits more clearly (dark brown) and displays a larger amount of metastatic cells in the lower part of the node (red arrows). Some metastatic cells can be detected in the upper part of the node (blue arrows) but deposits are less pronounced.

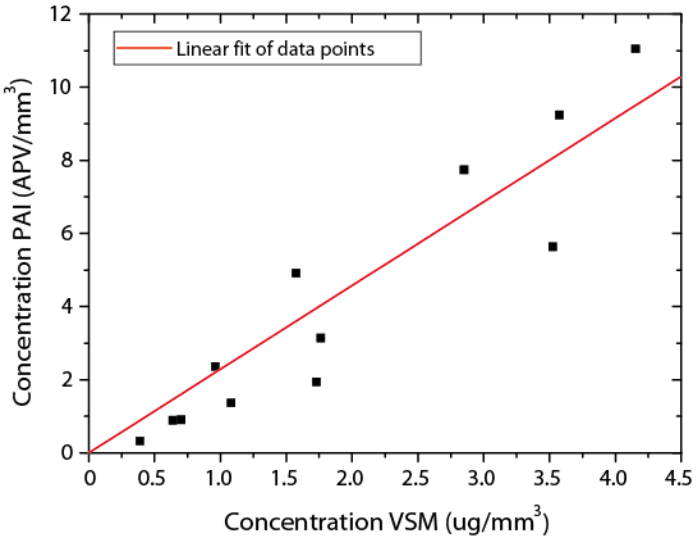

Figure 8. Correlation between the measured iron concentration with VSM and the calculated PA image contrast. Linear fit through 0,0 of the data points (red line) shows an linear correlation between the two (CC: 0.94, Root MSE: 1.3).

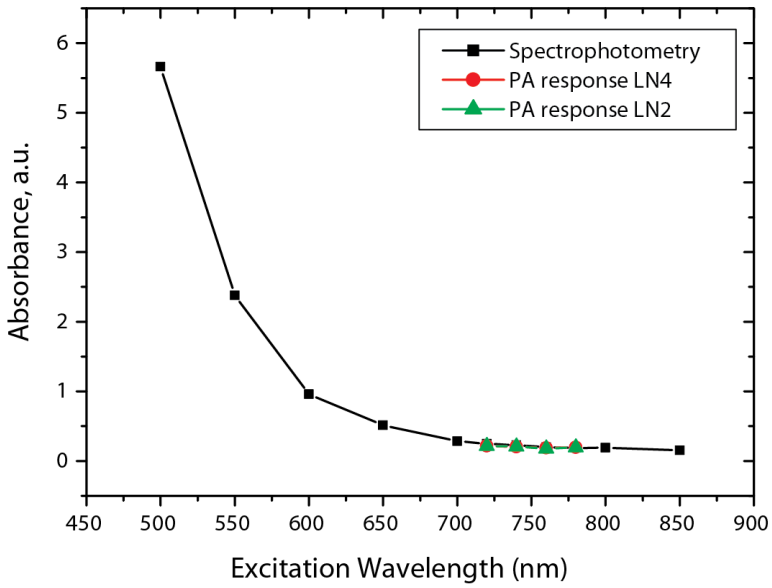

Figure 9. Correlation between the optical extinction of a SPIO dispersion measured with optical spectroscopy (black line) compared to the amount of PA response at 4 different excitation wavelengths (green and red line). Both the optical absorption and PA response are almost constant at the wavelength range from 720 to 780 nm. This constant absorption is not present in other biological chromophores, which might offer additional grounds to distinguish SPIO particles *in vivo*.

Control nodes	Iron concentration VSM (ug/mm^3)	PA contrast in image (mm^{-3})
1	2,9	13,0
2	3,5	9,6
3	4,2	15,6
4	3,6	15,0
Metastatic nodes	**Iron concentration VSM (ug/mm^3)**	**PA contrast in image (mm^{-3})**
1	0,4	0,8
2	0,6	2,5
3	1,0	5,4
4	0,7	3,8
5	1,6	8,4
6	1,1	6,8
7	1,8	7,5
8	1,7	6,5

Table 1. Measured SPIO concentrations and PA contrast within the individual nodes. Nodal numbers correspond to the numbering within the figures.